GEOPHYSICS, VOL. 81, NO. 1 (JANUARY-FEBRUARY 2016); P. 1–13, 10 FIGS., 2 TABLES.
10.1190/GEO2015-0186.1

Helicopter-borne transient electromagnetics in high-latitude environments: An application in the McMurdo Dry Valleys, Antarctica

Neil Foley[1], Slawek Tulaczyk[1], Esben Auken[2], Cyril Schamper[3], Hilary Dugan[4], Jill Mikucki[5], Ross Virginia[6], and Peter Doran[7]

ABSTRACT

The McMurdo Dry Valleys are a polar desert in coastal Antarctica, where glaciers, permafrost, ice-covered lakes, and ephemeral summer streams coexist. Liquid water is found at the surface only in lakes and in the temporary streams that feed them. Past geophysical exploration has yielded ambiguous results regarding the presence of subsurface water. In 2011, we used a helicopter-borne, time-domain electromagnetic (TDEM) sensor to map resistivity in the subsurface across the Dry Valleys. The airborne electromagnetic (AEM) method excels at finding subsurface liquid water in polar deserts, where water remains liquid under cold conditions if it is sufficiently saline, and therefore electrically conductive. Over the course of 26 h of helicopter time, we covered large portions of the Dry Valleys and vastly increased our geophysical understanding of the subsurface, particularly with respect to water. Our data showed extensive subsurface low-resistivity layers of approximately 150–250 m beneath higher resistivity layers, which we interpreted as freeze-concentrated or "cryoconcentrated" hypersaline brines lying beneath glaciers and frozen permafrost. These brines appeared to be contiguous with surface lakes, subglacial regions, and the Ross Sea, which could indicate a regional-hydrogeologic system, wherein solutes might be transported between surface reservoirs by ionic diffusion and subsurface flow. The presence of such brines underneath glaciers might have implications for glacier movement. Systems such as this, where brines exist beneath glacial ice and frozen permafrost, may exist elsewhere in coastal Antarctica; AEM resistivity is an ideal tool to find and survey them. Our application of TDEM demonstrates that in polar subsurface environments containing conductive brines, such a diffusive electromagnetic method is superior to radar surveying in terms of depth of penetration and ability to differentiate hydrogeologic conditions.

INTRODUCTION

In polar regions, particularly in Antarctica, mean annual temperatures well below freezing shape the dominant physical and chemical landscape properties. The McMurdo Dry Valleys (MDV) form the largest ice-free region in Antarctica with mean annual temperatures of −15° to −30°C (Doran et al., 2002). The Transantarctic Mountains block most ice from the East Antarctic Ice Sheet from entering several valleys, the largest of which open to the Ross Sea and are believed to have been fjords during the Miocene and Pliocene (Sugden et al., 1995). The MDV are an example of an extreme polar desert, with minimal precipitation and high rates of moisture loss through wind-driven ablation and sublimation (Doran et al., 2002). Despite the cold and arid climate, the MDV are one of the few places in Antarctica where liquid water can be found at or near the surface, either in ephemeral summer streams or perennially ice-covered lakes. As is typical of desert climates, many of the lakes have saline bottom waters (Lyons et al., 2005).

The lakes, streams, and climate of the MDV have been studied for decades as part of the National Science Foundation-funded Long

Manuscript received by the Editor 18 March 2015; revised manuscript received 28 September 2015.
[1]University of California, Earth and Planetary Sciences, Santa Cruz, California, USA. E-mail: ntfoley@ucsc.edu; stulaczy@ucsc.edu.
[2]Aarhus University, Department of Geosciences, Aarhus Denmark. E-mail: esben.auken@geo.au.dk.
[3]Sorbonne Universités, UMR 7619 METIS, UPMC Univ Paris 06, Paris, France. E-mail: cyril.schamper@upmc.fr.
[4]University of Wisconsin, Center for Limnology, Madison, Wisconsin, USA. E-mail: hilarydugan@gmail.com.
[5]Middlebury College, Department of Biology, Middlebury, Vermont, USA. E-mail: jmikucki@middlebury.edu.
[6]Dartmouth College, Environmental Studies Program, Hanover, New Hampshire, USA. E-mail: ross.a.virginia@dartmouth.edu.
[7]Louisiana State University, Department of Geology and Geophysics, Baton Rouge, Louisiana, USA. E-mail: pdoran@lsu.edu.

Term Ecological Research (LTER) program, which is partly a continuation of monitoring performed by the New Zealand Antarctic Program since the late 1950s. Our knowledge of the subsurface and any associated groundwater is limited to geophysical exploration done in preparation for the Dry Valley Drilling Project (DVDP) (McGinnis and Jensen, 1971; McGinnis et al., 1973) and the subsequent drilling effort (Decker and Bucher, 1977; McGinnis and Osby, 1977; Cartwright and Harris, 1981; Stuiver et al., 1981). Results from these investigations offer ambiguous evidence for subsurface water. Electromagnetic (EM) resistivity and active-source seismic investigations have been interpreted as being indicative of liquid brines trapped under relatively thin frozen ground (McGinnis et al., 1973). Based on a few such measurements near lakes, McGinnis et al. (1973) postulate that these brines are part of a "continuous hydrogeological unit" in the region. Thermal measurements from DVDP boreholes indicated that permafrost, broadly defined as any material that is perennially below 0°C but not necessarily devoid of liquid brine, was widely present in the MDV to depths up to almost 1000 m (Decker and Bucher, 1977), and therefore largely isolated the surface hydrologic features from any groundwater at depth (Cartwright and Harris, 1981). Since then, research on the MDV hydrologic system has focused on the contributions of water and solute transport in the active layer (Levy et al., 2011; Dickson et al., 2013; Toner and Sletten, 2013; Toner et al., 2013) and surface streams (e.g., Lyons et al., 2005). Surface hydrology research has flourished in part due to greater accessibility and the LTER research theme of investigating surface connectivity.

Studies of subsurface hydrology are often complicated by varying uses of the term "permafrost." Permafrost is commonly defined as ground that is perennially below 0°C (Ferrians et al., 1969; Cartwright and Harris, 1981; Osterkamp and Jorgenson, 2009), but some authors explicitly define it as frozen ground without liquid water or brine in pore spaces (e.g., Minsley et al., 2012). The distinction is important in areas where solute concentrations can significantly depress the freezing point of water, such as in the MDV. This paper uses the more common definition of permafrost as subzero-degree Celsius ground. Previous authors may have associated such permafrost with barriers to groundwater flow, but this is not necessarily the case, and this imprecision may have helped to discourage investigation of groundwater in the MDV after the early 1970s.

Due to increased environmental protection of the MDV as part of an Antarctic Specially Managed Area, permafrost drilling in the future will have to be undertaken sparingly and with due attention to environmental stewardship. Thus, low-impact geophysical techniques are necessary to investigate regional-subsurface hydrology and its connectivity to surface features and the coastal ocean. First used in the 1970s in the MDV, electric resistivity methods remain an effective way to investigate subsurface distribution of brines.

Transient electromagnetic (TEM) methods are known to be highly sensitive to electrically conductive targets, such as brine or wet clays, which return strong inductive secondary EM fields. Resistive geologic units, such as dry sand, ice, or frozen permafrost, give weaker responses, often close to ambient noise levels (Ward and Hohmann, 1988; Christiansen et al., 2006). For this reason, the TEM method and more generally, all induction EM methods have been intensively used for the mapping of conductive units. Hydrogeologic and resource applications of TEM include mapping clay-rich aquitards, which offer protections for aquifers (Palacky, 1987; Kirsch et al., 2003; Foged et al., 2014), seawater intrusion in coastal aquifers for water quality control and management (Kirkegaard et al., 2011; Teatini et al., 2011; Jørgensen et al., 2012) and mining exploration of highly conductive mineral deposits (Smith, 2014). Minsley et al. (2012) use frequency-domain EM to map permafrost above groundwater in arctic Alaska.

Because the MDV contain high-resistivity ice and low-resistivity brines, there exists a large EM-resistivity contrast between frozen ground and ground containing liquid brine (Dugan et al., 2015a; Mikucki et al., 2015). This paper presents results from the first airborne electromagnetic (AEM) survey in Antarctica, performed in November 2011 in select locales in the MDV, and it expands on the technical aspects of the AEM system, with comparisons to other techniques and past geophysical exploration. The survey was done using the SkyTEM system developed by the Hydrogeophysics Group at University of Aarhus (Sørensen and Auken, 2004), which also wrote accompanying data processing algorithms (Auken et al., 2009). AEM combines a large depth of investigation (DOI) with the mobility and high-spatial resolution afforded by helicopter-borne equipment (Sørensen and Auken, 2004). This AEM survey provides a regional-scale, high-resolution 3D representation of subsurface resistivity in MDV. It significantly expands the understanding of the subsurface geology and hydrology compared with the geophysical measurements made in the early 1970s. Numerous measurements of lake conductivity and the DVDP boreholes in the 1970s allow us to validate our data.

METHODS

Airborne electromagnetic

In the MDV survey, we used the SkyTEM system initially developed in the early 2000s for hydrogeological mapping (Sørensen and Auken, 2004). It is based on the time-domain electromagnetic (TDEM) method, which measures the secondary EM field induced in the ground after an abrupt turn-off of a pulsed primary electromagnetic field generated by a large transmitter loop several hundred square meters in area. The time decay of this secondary EM field is generally measured by an induction receiver coil (a compact solenoid of tens of square meters of effective area), which records the time derivative, or electromotive force, of the magnetic field. This measure is usually denoted as $\partial b/\partial t$ with units of $\mathrm{V/m^2}$ (the voltage measured between the two extremities of the receiver coil normalized by its area). In late times, after the primary field has decayed,

$$\frac{\partial b}{\partial t} = -\frac{I\sigma^{3/2}\mu_0^{3/2}a^2}{20\sqrt{\pi}}t^{-5/2}, \tag{1}$$

where I is the current, σ is the conductivity, μ_0 is the permeability of free space, a is the radius of the coil, and t is the time (Ward and Hohmann, 1988). Importantly, apparent conductivity can be determined as a function of time, giving a first overlook of the conductivity variations as a function of depth. This equation also highlights that measured $\partial b/\partial t$ decreases proportionally to $t^{-5/2}$, which means that the TDEM signal decreases by five orders of magnitude per two orders of magnitude in time. Usually two to three orders of magnitude of time are observed in practice, so an efficient TDEM measurement device needs to be able to record differences of electric

potentials that can be one billion times different in amplitude (from approximately 1 V down to μV).

Most recorded TDEM responses cover the equivalent frequency range from 10 Hz to approximately 300 kHz. The high-frequency content is used to invert for electric properties of the near surface at relatively high vertical resolution based on TDEM measurements made immediately after turning off the primary current in the transmitter loop. As time elapses, TDEM measurements provide information on electric resistivity at increasing depth. These later signals come from the lower frequency part of the spectrum leading to decreasing vertical resolution. There are practical challenges to acquiring near-surface and deep information due to the longer time required to shut down the higher primary current in the transmitter loop, which filters the highest frequency content, and due to the decreased signal-to-noise ratio (S/N) at late times.

Because ground TDEM response globally decreases as a factor of $t^{-5/2}$ and time windows for recording the secondary ground response span from approximately 10 μs to a few ms, there is a huge drop of signal level for a single TDEM sounding. If the moment (the product of current, loop area, and number of wire turns) in the transmitter loop is increased to improve the S/N for late observation times, the turn-off becomes longer and near-surface vertical resolution deteriorates. To tackle this issue, the SkyTEM system transmits current at low (LM) and high (HM) transmitter moments to achieve an improved broadband system. The LM is optimized for near-surface mapping by providing higher frequency content via its faster turn-off, whereas the HM is optimized for deep investigation by increasing the ground TDEM response above the noise level at late times via high current and multiple turns (Figure 1a).

AEM compares favorably with the more commonly used radio echo sounding (RES) technique for creating regional-scale geophysical data sets in areas where low-resistivity material is widespread. Both techniques use the time-variable EM field, but in the EM induction approach, the field varies slowly enough for its propagation part to become negligible compared with the diffusion term (i.e., the second-order time derivative of the field strength is negligibly small). EM induction frequencies are typically a few to several orders of magnitude lower than are RES frequencies, resulting in wavelengths much larger than the skin depth of field penetration (Zhdanov, 2009). The high frequencies used in radar applications mean that the second time derivative of field strength is nonnegligible and its propagation is described by the wave equation. Under conditions of low conductivity, radar waves have small wavelengths relative to their skin depths. The skin depth δ of an EM field (frequency $f \sim < 10^5$ Hz) is proportional to $\sqrt{(\frac{\rho}{f})}$, so low-frequency fields or high-resistivity materials lead to large skin depths (Sharma, 1997). For radar (frequency approximately $>10^7$ Hz), $\delta \propto \rho$; radar is therefore sensitive to changes in the dielectric constant and is strongly attenuated in low-resistivity materials (Sharma, 1997). Consequently, although the higher frequency radar has higher spatial resolution than do EM induction methods, radar waves penetrate less deeply into the ground than diffusive EM fields, particularly when conductive materials are present. The EM frequency can be tuned to penetrate through some thickness of conductive materials, with more conductive material requiring lower frequency fields (Sharma, 1997).

The SkyTEM504 system flown for our MDV survey has a total weight of approximately 500 kg, a transmitter area of approximately 500 m^2, four transmitter coil, turns and a current for the HM moment of 95 amps. The resulting maximum DOI is approximately 350 m depending on the conductivity of the subsurface. The transmitter frame was assembled on the sea ice near the U.S. McMurdo Station. Figure 2a shows the first calibration lifts by the Bell 212 helicopter.

Data acquisition

Average flight altitude of the survey was approximately 35 m above the ground surface. Flight lines were spaced by 200–400 m (Figure 3), the average flight speed was 55 km/h, and the effective sounding spacing along the lines was approximately 50 m after averaging three raw data sets into one. TEM data used in this study were collected between 13 μs and 8 ms from the beginning of the current turn-off, with the beginning of this time record corresponding to 8 μs after the end of the transient response ramp. Each sounding corresponds to two consecutive LM and HM pulses linked to one GPS position and constitutes a dual-moment sounding curve (Figure 1b). The LM part of the curve has a stack of 256 transients (each one lasts approximately 2 ms including the period of injection and the period over which the secondary EM response is measured), and the HM has a stack of 64 transients (each one lasts approximately 16 ms). Additional software stacking is carried out during processing to improve the S/N at late measurement times. Two lasers mounted on the frame measure its altitude during flight. The frame pitch and roll are recorded using two tilt meters also mounted on the frame. The positions of all these devices are indicated in Figure 2b. Data were kept up to a maximum altitude of 70 m above the surface, and the frame pitch and role rarely exceeded ±10°.

Data processing

The main processing steps follow the work of Auken et al. (2009) and are described here briefly. Corrections to compensate the pitch and roll of the loop were done automatically via continuous tilt measurements during the survey. Altitude records from the lasers required no manual corrections because there is no vegetation on the surface of the MDV.

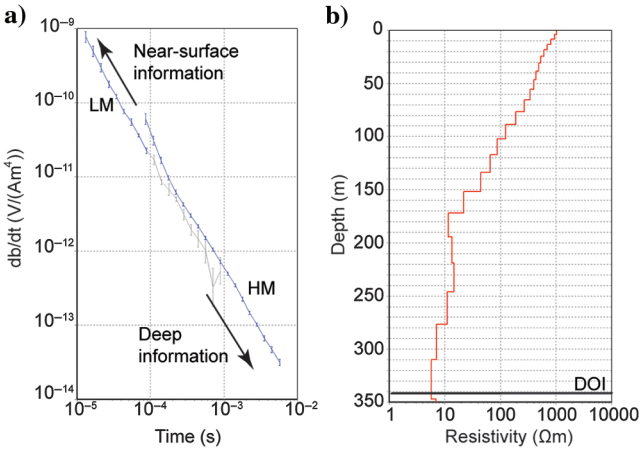

Figure 1. (a) Typical dual-moment TEM curve with LM and H (the two curves are normalized by the moment) and (b) the corresponding 29-layer resistivity model with its estimated DOI. The sounding position is indicated on the profile shown in Figure 4.

Prior to the survey, the AEM system was calibrated at the national reference site in Denmark to correct the signal amplitude and time shifts (Foged et al., 2013). For the calibration of the system, the estimated time shift is less than −0.7 μs for LM and −3 μs for HM, and there is an amplitude shift factor of 0.92. These shifts have little effect on the data, but they ensure that the measurements are calibrated to the best possible accuracy.

Two main precautions for the sounding curves were considered:

1) Early times at LM (Figure 1a): There was still some residual current in the transmitter loop at the first times recorded just after the turn-off. This system response is called the *coil response (CR)* and is measured with the AEM system flown at high altitude (>1000 250 m) where no ground response can be measured. The CR was later removed during data inversions (Schamper et al., 2014). In the MDV, some areas were so resistive within the depth of signal penetration that only CR data were recorded. Correction for the CR effect during data inversion is important to avoid a misleading interpretation of early times (Schamper et al., 2014) resulting in the location of false conductive or resistive layers in the shallow subsurface.
2) Late times at LM and HM (Figure 1a): In areas where no conductive layers are present in the subsurface, many late time gates were below the noise level and were removed from the data set. If noisy late times are kept, it results in fictitious deep conductive layers. In many areas of the MDV, only a few gates remained after this cleaning process. When the number of remaining gates was too low (<4), these data were removed before inversion.

A gate-by-gate plot of a typical section across Lake Fryxell is shown in Figure 4a. The gates for each TEM sounding are shown along the flight line, illustrating the different levels of signal detected. As shown, (1) LM and HM have a high signal above Lake Fryxell, which contains brackish water; (2) just the HM signal is high outside of the lake, where there is only a deep conductor (permafrost with brines) with a resistive cover (permafrost with no liquid water in pore spaces) as seen on the northwestern side of the profile (Figure 4a); and (3) on the most northwestern part of the profile, the entire signal drops and HM has only a few gates remaining indicating very thick, high-resistivity permafrost and no conductive layers within the entire range of depth penetration.

To maintain good near-surface resolution and to improve the S/N at late times, trapezoidal filters (which average early times less than late ones) with stacking windows enlarging with the time delay were applied. This way there is no additional loss of lateral resolution in the near surface with a narrow stack window (6 s for first gates of MCM survey), and there is a reduction of noise with a wider window at late times for a better DOI (up to 20 s for the latest gates) (Auken et al., 2009).

Data inversion

Modeling and inversion of the AEM data were carried out with the AarhusInv program (Auken et al., 2014; Kirkegaard and Auken, 2015) using the Aarhus Workbench. We used the spatially constrained inversion scheme (Auken and Christiansen, 2004; Viezzoli et al., 2008) providing a quasi-3D resistivity model of the ground with local vertical forward and derivative calculations. Each sounding position corresponds to a local 1D resistivity model, which is linked by spatial constraints to its neighboring soundings. Those constraints ensure continuity between adjacent soundings. For this

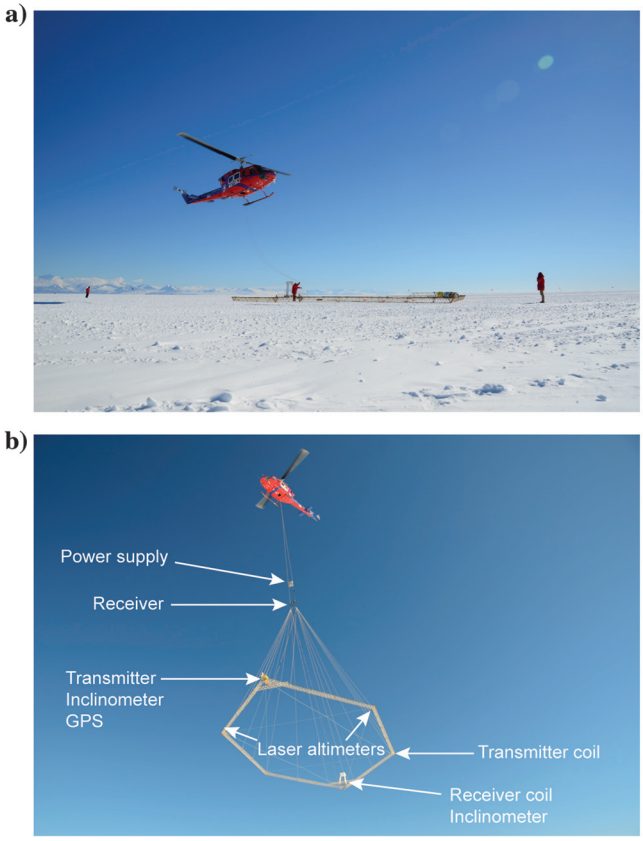

Figure 2. (a) The SkyTEM504 frame being lifted by a Bell 212 helicopter on the sea ice outside McMurdo Station, 2011, and (b) SkyTEM504 system in the air.

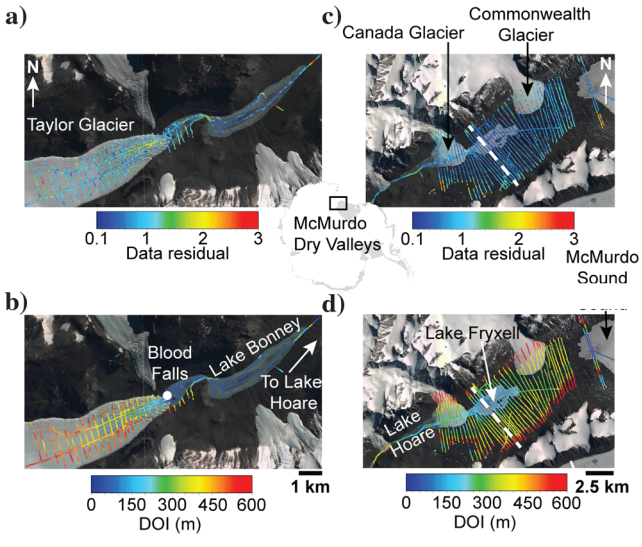

Figure 3. Flight lines after data processing with data residual for (a) Taylor Glacier (TG) and (c) Taylor Valley (TV), and DOI for (b) TG and (d) TV as colored points. The dashed white line corresponds to the profile shown in Figure 4.

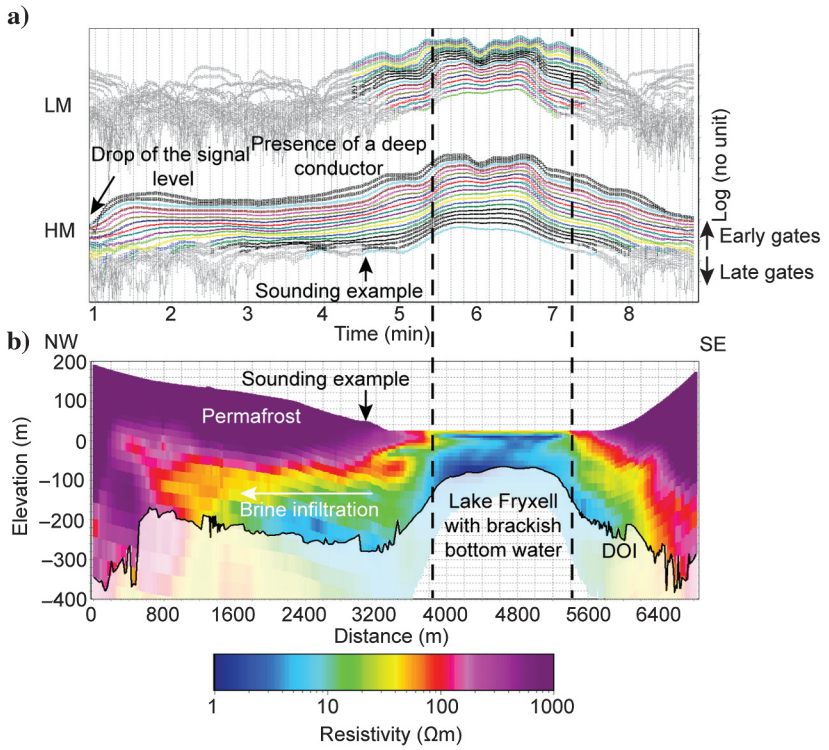

Figure 4. Flight line across Fryxell Lake and its surroundings (white dashed line in Figure 3): (a) processed gate-by-gate data section with LM and . Too-noisy gates are fainted and (b) the corresponding 29-layer resistivity model section obtained after the inversion. The dark line indicates the DOI. The location of the sounding example shown in Figure 1 is indicated.

inversion, lateral constraints were set to a factor of 1.35 and increased rapidly beyond a radius of 20 m. This means that resistivity values can vary within 35% from one sounding to another. These constraints are not strict and do not forbid sharp changes if the fitting with the data requires it. Each vertical resistivity model consists of 29 layers with thicknesses starting from 1.5 to 4 m near the ground surface and increasing logarithmically until a depth of 350–650 m (Figure 1b), depending on the overall vertical resistivity distribution of each subarea. A many-layered inversion was chosen over a few-layered inversion scheme because the former eliminates the need to make an initial guess on the number of geologic layers across the survey area. The change in the number of geologic layers is illustrated in Figure 4b: Only one overall very conductive layer can be detected above Lake Fryxell, whereas varying levels of resistivity within the permafrost can be observed around the lake.

The smooth inversion scheme requires the consideration of vertical constraints between neighboring layers to ensure nonerratic resistivity models. For the MDV data set, the vertical constraints are set loose (factor of 1.6) in order not to overly smooth the sharp transitions (e.g., between glacier ice and subglacial brine). Despite this, smoothing in the presented inver-

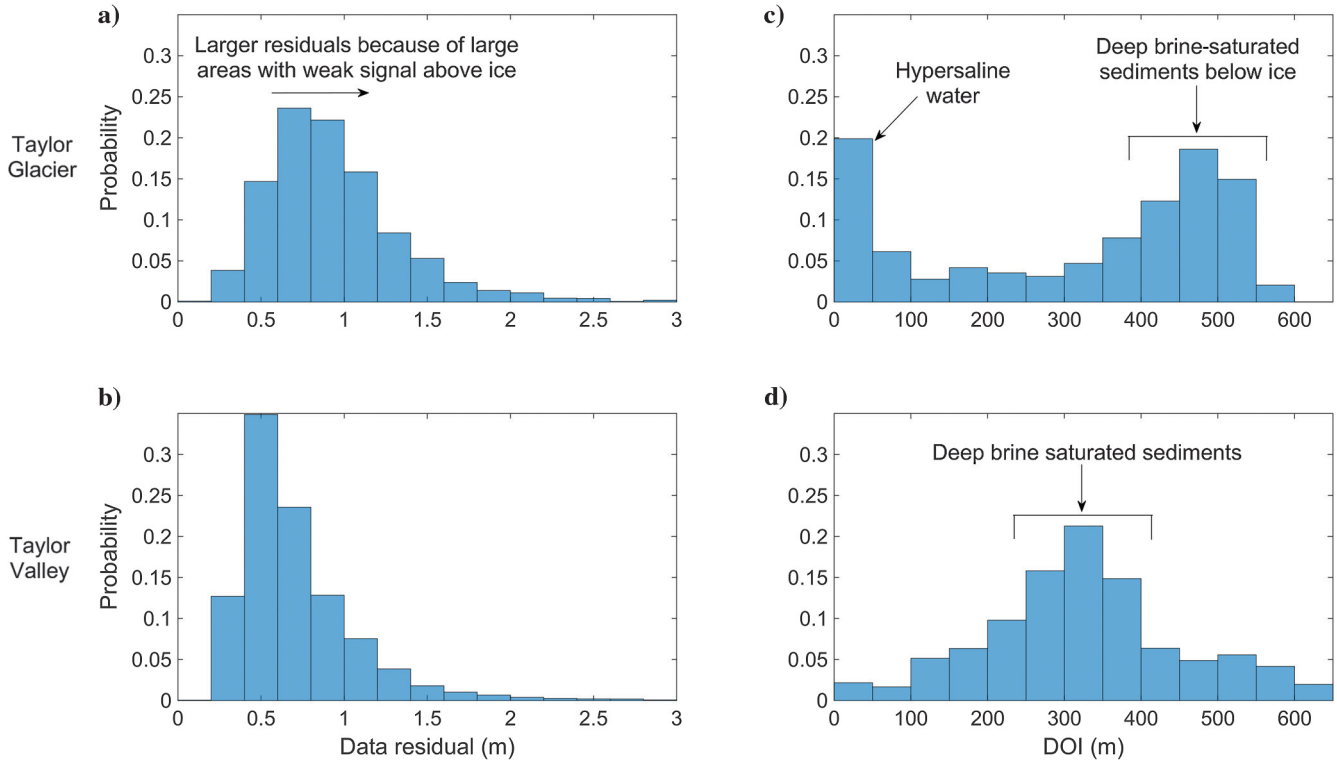

Figure 5. Histograms of DOI and data residuals for TG and TV.

sion results is still present. It is related to the resolution obtainable with the diffusive induction EM method. Sharper boundaries can be mathematically obtained (Vignoli et al., 2015), but this must be constrained by other data (e.g., RES and boreholes) to minimize the inherent equivalence issues (where different ground models explain the acquired data equally well). Combining different geophysical data sets with the AEM data to get sharper boundaries is beyond the scope of the present paper, but it may be included in future interpretations.

The inversion algorithm uses a forward modeling code, in which all parameters of the acquisition device are modeled to avoid misinterpretation of TDEM data (Christiansen et al., 2011): the waveform of the current injected in the transmitter loop; low-pass filters of the system; and altitude of the system, which is considered as an inversion parameter constrained to the value measured by the laser.

Data and inversion quality control

Several parameters are checked during quality control of data and inversions. Data processing is quality controlled by checking the following: (1) the GPS positions, which need to be consistent with the planned survey and the background GIS map; (2) the continuity of the altitude measurements (20 points every second with a laser); (3) any abnormally high tilt values exceeding $\pm 10°$; (4) the presence of too-noisy gates (normally fainted as in Figure 4a), which could indicate a nonoptimal definition of the noise level (approximately 5.10^{-8} V/m^2 at 1 ms for this survey).

The main inversion parameter checked during quality control is the data-fit residual, which is the difference between the model output and the field data, normalized by the standard deviation of the data. A data-fit residual of less than one indicates a good fit of the estimated resistivity model into the field data within the observational error estimated using the trapezoidal stack window. An abnormally high residual can have several causes: The noise cleaning process was not sufficient, spatial constraints were too strong to allow resistivities to change enough during the iterative inversion, and/or considered system parameters are badly defined. The overall data residual of an explored area should have a value of less than one. In the case of the MDV survey, the data residuals are low where brine is present (Lake Bonney in Figure 3a and Lake Fryxell in Figure 3c), and they become more erratic where the signal is close to the noise level above resistive areas, such as thick, brine-free permafrost or shallow bedrock (the sides of Taylor Valley [TV] in Figure 3c) or glacial ice of more than several hundred meters in thickness (e.g., upstream on Taylor Glacier [TG] in Figure 3a). Overall, the data residual for the study area is less than 1.0. A histogram of residuals for TG (Figure 5a) shows a globally larger data residual than in our TV data (Figure 5b), although most of it remains at less than 1.5. This is due to the large areas covered by thick, high-resistivity ice of TG, which results in a weak secondary EM response. This observation is also illustrated with the statistics in Table 1.

Table 1. Statistics on DOI estimation and data residuals for TG and TV.

	DOI TG (m)	Data residual TG	DOI TV (m)	Data residual TV
Minimum	31.9	0.14	29.8	0.11
Maximum	597.	12.7	650	13.0
Mean	315	0.97	328	0.74
STD	187	0.57	130	0.55
Median	384	0.87	325	0.62
% < 1	—	63.7	—	83.6
% <1.2	—	79.4	—	91.1
% <1.5	—	90.6	—	96.0
% < 50 m	19.9	—	2.15	—
% >300 m	60.4	—	59.4	—

The estimated resistivity models are automatically analyzed at the end of the inversion to evaluate the DOI (Christiansen and Auken, 2012). This sensitivity analysis considers the cumulated response of the data to each layer's resistivity from the deepest layer:

$$S_j = \sum_{j=M,-1}^{k} \frac{\sum_{i=1}^{N} \frac{G_{ij}}{\Delta d_i}}{t_j}, \tag{2}$$

where S_j is the cumulated sensitivity from the deepest layer to layer j, M is the total number of layers, N is the total number of data points, t_j is the thickness of layer j, $G_{ij} = \partial \log(d_i)/\partial \log(\rho_j)$ is the sensitivity of data point i to the resistivity of layer j, and Δd_i is the standard deviation of data point d_i. The total number of layers M can be larger than the number of layers of the inverted model (resistivity is repeated within each inverted layer), to get a finer estimation of the DOI. Once the cumulated sensitivity S_j reaches a threshold value, which is fixed based on the experience with field data and cross comparisons of models obtained from different methods Christiansen and Auken (2012) estimate a threshold value within the range 0.6–1.2), the DOI is reached.

This sensitivity analysis provides the basis for fading of the resistivity sections below a depth, from which resistivity values have almost no impact on the measurements (see sounding example of Figure 1b). DOI estimation is important to avoid overinterpretation of deep conductors whose presence may be entirely due to the numerical optimization or noisy data inadvertently left in the late part of the TDEM signal. In the present survey, the DOI is less than 50 m above brackish to hypersaline lakes (Lake Bonney in Figure 3b and Lake Fryxell in Figure 3d), and it reaches approximately 350–400 m, where good conductors are located below high-resistivity layers, and there is still a representative and reliable signal. Where few gates remain with a poor signal, indicating that only highly resistive formations (greater than 1000 Ωm) are present, the DOI estimation can go beyond 400 m (top of TG in Figure 3b and sides of TV in Figure 3d). A histogram of DOI values for TG shows a large portion of values smaller than 50 m (Figure 5c). This is due to the presence of hypersaline water close to the snout of the glacier. A large portion of DOI values for TG are also greater than 400 m, likely due to the presence of a deep subglacial conductor beneath high-resistivity glacial ice. Figure 5d also shows DOI values in TV are not as high as in TG, with 350 m being the most common. Numerical statistics are available in Table 1.

RESULTS

We collected data from approximately 300 km^2 of the MDV, with the best coverage over eastern TV (Figure 3a and 3b) and the lower

4 km of TG in western TV (Figure 3c and 3d). This is the most complete regional-scale subsurface geophysical data set of any type collected in the MDV. Its wide coverage and deep DOI allow us to expand upon work done at smaller scales by previous researchers and complement work done with different geophysical techniques.

Prior to our survey, some of the most complete subsurface geophysics in the MDV came from limited measurements from the 1970s. McGinnis et al. (1973) use active seismic refraction in conjunction with Schlumberger and Wenner DC resistivity arrays to investigate the subsurface in small areas near potential DVDP borehole sites. At the west end of Lake Fryxell, near the eventual site of DVDP borehole number 7, they measure a transect across a narrow part of the lake using two seismic stations and six resistivity stations. From the data, they generate a model (Figure 6a) that presents their seismic and geoelectric interpretations down to approximately 40 m below the surface. Their models indicate that there are widespread deep areas of relatively lower resistivity (<400 Ωm) covered by high-resistivity material (1000–10,000 s of Ωm) on either shore. They interpreted this situation as sand and gravel saturated with unfrozen water beneath frozen permafrost, which they speculated could be connected to a regional aquifer beneath frozen permafrost.

In the Fryxell Basin, our data produced a model that is consistent with their inferences but much more detailed and in 3D. The AEM system is able to constrain resistivity at much greater depths than the techniques used by McGinnis et al. (1973); at Lake Fryxell it measures more than 200 m below their deepest measurements. Our regional-scale measurements produce reasonable results: We detect low-resistivity material (<100 Ωm) at the lake where there is brackish water, surrounded by with higher resistivity material (100–1000 s of Ωm) on the shores where frozen ground is expected (Figure 6b). As do McGinnis et al. (1973), we measure the highest resistivities north of the lake. Our data show that the low-resistivity area extends laterally underneath the shallow frozen permafrost for hundreds to thousands of meters, representing a large fraction of the valley's width, and down at least 200 m without indication of any clear increase in resistivity until the survey reaches the DOI limit.

Unfortunately, the DVDP borehole drilled in the Fryxell Basin, DVDP 7, penetrated, with difficulty, a mere 11.2 m before the borehole collapsed (McGinnis and Osby, 1977), and it consequently yielded little information, so it is not very useful for comparison with our measurements. Further east, DVDP 11 near Commonwealth Glacier achieved a depth of approximately, at which point it lost drilling fluid (McGinnis et al., 1982), potentially indicating a permeable aquifer. An AEM sounding at the same location shows a sharp drop in resistivity between depths of 200 and 275 m coincident with sharp increases in salinity within marine sediments (Figure 7). This occurs over a range of temperatures (approximately −10°C to −6°C) consistent with temperatures at which MDV brines could exist: The saline bottom waters of Lake Bonney are −5.3°C (Spigel and Priscu, 1996); water exits Blood Falls, a hypersaline discharge at the terminus of TG, at −5.6°C (Mikucki et al., 2009); and Hubbard et al. (2004) predict basal temperatures beneath TG, where brine is present, to be at most −7.8°C further east DVDP 10 filled with 72 ppt brine at approximately 180 m deep (McGinnis et al., 1982) and approximately −6°C (Decker and Bucher, 1982),

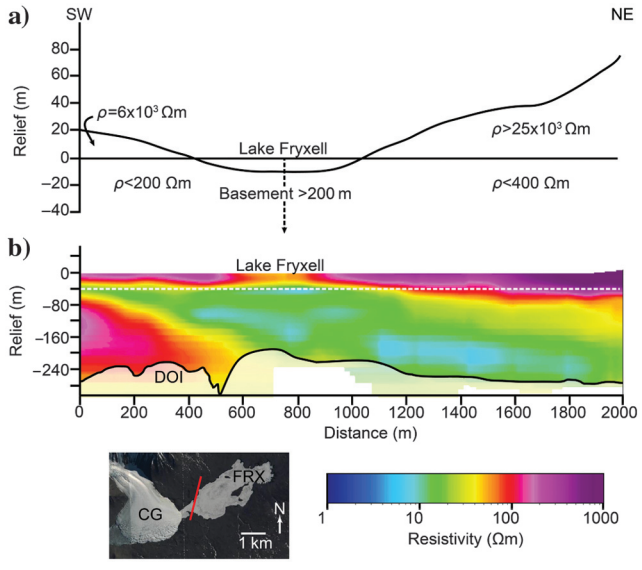

Figure 6. Profile across Lake Fryxell: (a) simplified version of McGinnis et al. (1973) model and (b) our model, with the maximum depth of the 1973 model marked by the dashed white line. Inset: map of area; CG, Canada Glacier; FRX, Lake Fryxell; and the red line marks the profile.

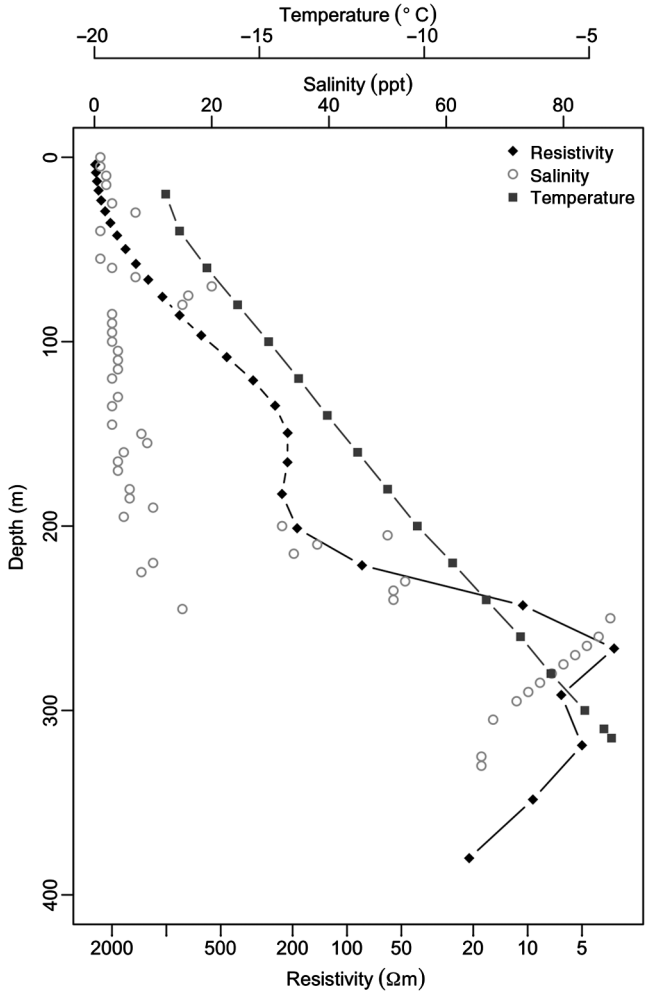

Figure 7. AEM data compared with DVDP 11 borehole temperatures (Decker and Bucher, 1982) and salinity (McGinnis et al., 1982). The DVDP 11 borehole location is marked in Figure 8.

indicating that there can be at least localized areas of hypersaline brines at depth within permeable sediments.

Regional cross section

A regional-scale view shows that the deeper layer of low resistivity measured in the cross section at Lake Fryxell (Figure 6b) is representative of the eastern portion of TV. At an elevation of –150 to 250 m, low-resistivity material is widespread throughout the lower reaches of the valley from Canada Glacier to the Ross Sea (Figure 8). The maximum depth of Lake Fryxell is approximately 20 to 250 m, therefore, resistivities at −150 to 250 m are well within sediments and bedrock beneath the lake bottom. The extent of this low-resistivity zone far exceeds the shores of Lake Fryxell, indicating that this represents a region of liquid groundwater that is outside the thermal influence of Lake Fryxell's talik, and therefore it is a truly regional aquifer. About half of the measurements taken in eastern TV at all depths have resistivities 100 Ωm or less, suggesting widespread brines. This potential aquifer may connect at depth with the Ross Sea, particularly in two "channels" of low-resistivity material that are visible on the north and south edges of Coral Ridge (Figure 8), an otherwise high-resistivity moraine complex from the last glacial maximum expansion of the Ross Ice Shelf (Hall et al., 2000) that separates TV from the Ross Sea.

Radio echo sounding and airborne electromagnetic

RES has been used infrequently in the MDV. Due to the labor involved with operating a ground-based unit, RES has typically been used to investigate small-scale features in the MDV, such as possible delta deposits and moraines (Arcone et al., 2000; Arcone, 2002), dunes (Bristow et al., 2010), lake ice (Dugan et al., 2015b), or glacial accumulation zones (Arcone and Kreutz, 2009; Shean and Marchant, 2010; McKay et al., 2014). We are aware of only one regional-scale airborne RES investigation (Holt et al., 2006), which was used primarily as a calibration exercise for potential future use of RES on Mars.

Compared with most of the RES measurements made in the MDV, AEM observes a far deeper domain. For example, Arcone et al. (2000) use 100-MHz radar at central Coral Ridge, to trace slightly dipping reflectors to a depth of 23 m, with implications for the emplacement history of the drift. At the same location on Coral Ridge, our AEM survey was able to measure up to 300 m below the surface. It detected large areas of low resistivity at depth beneath extremely high-resistivity material in the center of Coral Ridge, potentially stranded ice (Figure 9). There is a gap in the AEM data coverage between Coral Ridge and the Ross Sea, but the available data are suggestive of a deep connection between the Ross Sea and TV beneath Coral Ridge (Figures 8 and 9); this feature was not detected in radar or DVDP borehole logs (Powell, 1981).

Low-frequency radar (10–100 MHz) is commonly used to measure the basal topography of glaciers (e.g., Berthling et al., 2000; Isaksen et al., 2000; Degenhardt and Giardino, 2003; Hubbard et al., 2004; Engel et al., 2012), whereas a shorter wavelength (100–400 MHz) is used when high resolution is required (e.g., Fukui et al., 2008; Sold et al., 2014). Because the speed of EM waves in ice is in the range of 0.167 0.169 m.ns^{-1}, which adds some uncertainties depending on the value chosen), the vertical resolution (about a quarter of the radar wavelength) ranges from approximately 4–250 m at 10 MHz to 0.1 m at 400 MHz. Hubbard et al. (2004) use 10-MHz radar to image the lower part of TG, which terminates in Lake Bonney at the western end of TV. Based on strong basal reflectivity, they infer the presence of a liquid water reservoir stored in an overdeepening located 3–6 km from the glacier terminus. Thermal modeling indicated that the bed was everywhere below the pressure melting point of fresh water, leading Hubbard et al. (2004) to conclude that to remain liquid, such water must be hypersaline brine. Because AEM is sensitive to subsurface fluid salinity and can cross thicker layers of brine than radar by virtue of its larger skin depth, it offers a natural complement to radar for testing the scenario proposed by Hubbard et al.(2004). AEM's ability to measure through greater thickness of brine allows for

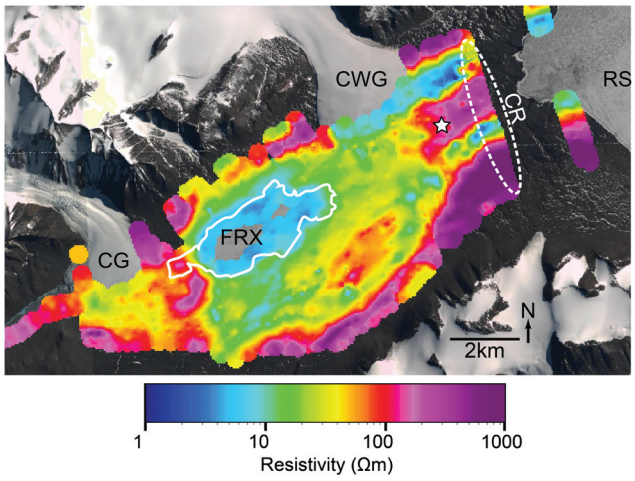

Figure 8. Resistivity at −150 m elevation. The solid white line indicates the surface expression of Lake Fryxell (FRX) and the dashed white ellipse marks the general location of Coral Ridge (CR). The star marks the location of DVDP 11. CG, Canada Glacier; CWG, Commonwealth Glacier; and RS, Ross Sea. There are no data in central Lake Fryxell because this is below the DOI at this location.

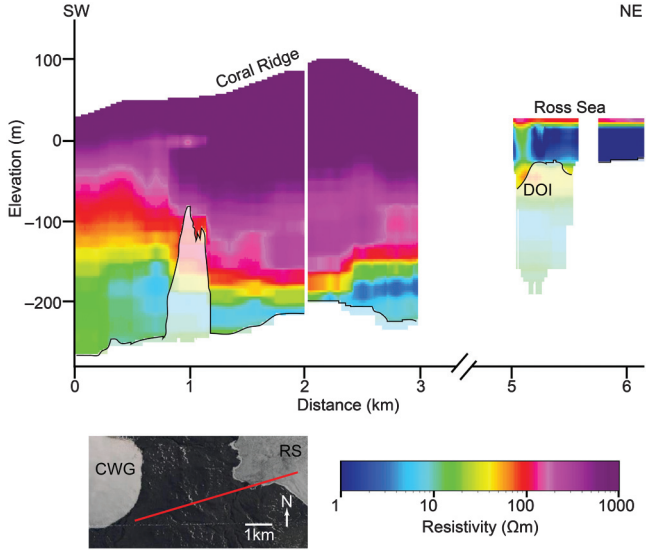

Figure 9. Resistivity profile across Coral Ridge. The *x*-axis is (distance) shortened over section of missing data. Inset, map of area; CWG, Commonwealth Glacier; and RS, Ross Sea.

more quantitative estimates of volume and salinity. We detect a horizontally continuous unit of low-resistivity material beneath the center of TG, which is present from its terminus in Lake Bonney until it is masked by the DOI 5–6 km up-glacier (Figure 10). In the up-glacier reaches of our profile, AEM cannot penetrate through as much ice as the radar used by Hubbard et al. (2004) (approximately 300–250 m with AEM versus approximately 450–250 m for GPR), but we do see spatial patterns of resistivity consistent with an overdeepening filled with low-resistivity material that is distinguishable from the extremely high-resistivity glacier ice. Based on this low resistivity, it has been interpreted as hypersaline brine (Mikucki et al., 2015), which is consistent with the high salinity measured in Blood Falls (Keys, 1979; Lyons et al., 2005; Mikucki et al., 2009), a hypersaline surface discharge at the terminus of TG (Figure 3b), and with the hypersaline bottom waters of Lake Bonney (Spigel and Priscu, 1996). A greater DOI from a higher moment transmitter would allow investigation farther up TG and constrain the size of this subglacial reservoir. Based on the presently available data, it is estimated that the volume of subglacial brine-saturated sediments is at least 1.5 km^3, which assuming a conservative estimate of the porosity at 12%, represents a volume of liquid water equivalent to the combined volume of the largest TV lakes (Mikucki et al., 2015).

DISCUSSION

This mapping of permafrost, glaciers, and subsurface liquid brine using AEM in the MDV demonstrates the potential applicability of this technique for future investigations in Antarctica and the Arctic, where regional-scale geophysical data sets will have impacts across disciplines. The effects of climate change and resultant feedbacks are predicted to be the most extreme at high latitudes (IPCC, 2007). Changes in surface and near-surface polar environments may trigger climate feedbacks, such as methane release from warming permafrost (Zimov et al., 2006; McGuire et al., 2009; Paytan et al., 2015) and from beneath retreating ice sheets (Wadham et al., 2008, 2012). Polar ice sheets may become important contributors to global sea level rise as the climate warms (e.g., Joughin et al., 2012).

Subsurface liquid water in particular plays an outsized role in high polar environments. Liquid water beneath glaciers and ice sheets is an important factor controlling glacier motion (Kamb, 1987; Creyts and Schoof, 2009; Winberry et al., 2011). However, TG is considered to be a cold-bottomed glacier, whose movement can be explained entirely by internal deformation (Kavanaugh and Cuffey, 2009; Petit et al., 2014). The widespread low-resistivity area detected beneath TG, which is consistent with hypersaline brine, may require this model to be reevaluated in light of unexpectedly abundant basal fluids. Other coastal glaciers in Antarctica may similarly have saline brines lubricating their bases or modifying the rheological properties of their basal ice, which would otherwise be too cold to contain liquid freshwater.

Antarctic subsurface liquid water has been shown to provide a viable habitat for microbes in an environment that is otherwise inhospitable (e.g., Christner et al., 2014). Antarctic briny aquifers may provide the best terrestrial analogs for potential subsurface habitats on Mars (Gilichinsky et al., 2003, 2007; Mikucki et al., 2015). Ancient water exiting from beneath TG at Blood Falls contains an assemblage of microbes using metabolic pathways enabling them to survive in an environment that may be analogous to a Snowball Earth refugium (Mikucki and Priscu, 2007; Mikucki et al., 2009), and conditions beneath frozen permafrost in the MDV may be similar. Groundwater may transport nutrients throughout the subsurface, providing important limiting nutrients, such as iron, to the coastal ocean (Wadham et al., 2013; Mikucki et al., 2015).

In a matter of days, the AEM system increased our understanding of subsurface water in the MDV more than decades of prior geophysical surveying and borehole investigations. Our results are broadly consistent with past geophysical investigation, but because our data cover a larger area and penetrate deeper into the surface, they yield a more comprehensive regional picture of subsurface conditions. We interpret the areas of low resistivity underneath TG and eastern TV as a large reservoir of liquid hypersaline brine stored within sediments. Unlike previous methods, we covered enough of TV to demonstrate the continuity of this brine over large parts of the valley, including likely hydrologic connectivity to the lakes through taliks and to the ocean beneath Coral Ridge. Geochemical studies of MDV lakes conducted over the last several decades have tended to discount the importance of deep groundwater flow into and out of the lakes (e.g., Poreda et al., 2004; Lyons et al., 2005), but the presence of such a large subsurface brine reservoir should motivate reevaluation of this assumption. The origin of the salts in MDV lakes is complex and believed to be variable for each lake (Lyons et al., 2005), but the brines beneath the surface may be more likely to share a common heritage. In the northern hemisphere, cryogenic processes have been invoked to explain the presence of shield brines (Herut et al., 1990; Starinsky and Katz, 2003). In the MDV, cryogenic processes may continue to occur in the subsurface, as permafrost freezes in response to the draining of Lake Washburn or as saline waters exit TG from an overdeepening through colder near-surface ice. The DOI of the AEM device is well suited to the scale that continuing freezing may occur over. A Stefan condition estimate (depth of freezing, $z = D\sqrt{t}$, where D is a constant between 1 and 5 that reflects the thermal properties of permafrost, after Osterkamp and Burn, 2003) suggests that permafrost growth due to the draining of Lake Washburn around the LGM

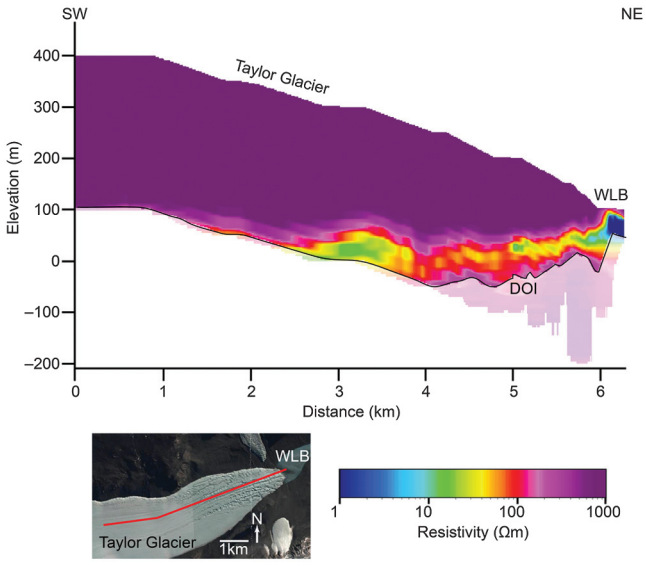

Figure 10. Profile along length of TG. Inset, map of area; WLB, West Lake Bonney. Blood Falls is at the terminus of TG in WLB.

(Hendy, 2000) should range from approximately 100 to 500 m. This is consistent with our measurements in Lower TV showing markedly decreased resistivity approximately 150 250 250 m below the surface.

Based on resistivity recorded at the site of DVDP 11, liquid brines in TV could exist at temperatures as cold as −10°C (Figure 7). Although ground at this temperature fulfills the definition of permafrost, it is not a hydrologic barrier equivalent to frozen permafrost. Indeed, it could contain a large fraction of pore space filled with water. Archie's (1950) law, an empirically determined relationship between bulk resistivity and porosity, can be used to estimate porosities in brine-saturated sediments. A simplified form is

$$\varphi = \left(\frac{\rho_0}{\rho_b}\right)^{-1/m}, \quad (3)$$

where φ is the liquid brine fraction, ρ_0 is the bulk measured resistivity of the formation, ρ_b is the resistivity of the brine, and m is a cementation exponent that reflects properties of the pore network and typically ranges from 1.4 to 2.8. Because the resistivity of the brine is not known and a cementation exponent for permafrost has not been determined, we calculated a range of possible porosities given reasonable values (Table 2). Based on moderate values (ρ_b equal to water at the hypersaline bottom of West Lake Bonney and $m = 2$, a value often used for sandstone) a measured resistivity of 10 Ωm (7% of measurements) could have an unfrozen brine fraction of 14.5%.

Table 2. Porosities calculated from resistivities for various possible scenarios. Lower values of formation factor *m* indicate less tortuous pore connections; *m* = 2.0 is a middle-range value. Seawater is probably a reasonable salinity upper bound, and Vida brine represents an extreme lower bound. Bottom West Lake Bonney water reported in Mikucki et al. (2015) and Lake Vida Brine reported in Dugan et al. (2015). Vida brine is liquid at −13.4 °C.

Porosities Determined from Resisitivity (%)

formation factor m = 1.5		ρ_b (Ωm) Seawater (−1.9 °C) 0.36	Bottom WLB 0.21	Vida Brine 0.15
ρ_0 (Ωm)	1	50.6	35.3	28.2
	10	10.9	7.6	6.1
	100	2.3	1.6	1.3

formation factor m = 2.0		ρ_b (Ωm) Seawater (−1.9 °C) 0.36	Bottom WLB 0.21	Vida Brine 0.15
ρ_0 (Ωm)	1	60.0	45.8	38.7
	10	19.0	14.5	12.2
	100	6.0	4.6	3.9

formation factor m = 2.5		ρ_b (Ωm) Seawater (−1.9 °C) 0.36	Bottom WLB 0.21	Vida Brine 0.15
ρ_0 (Ωm)	1	66.5	53.6	46.8
	10	26.5	21.3	18.6
	100	10.5	8.5	7.4

AEM has significant potential for further scientific investigations in coastal environments of Antarctica and the Arctic. Polar environments, where water commonly exists as a solid near the surface but can be liquid at depth, exhibit a range of resistivities that spans several orders of magnitude, making geophysical identification easy. Brines enhance this effect, but resistivity has been used to similar effect in freshwater systems in the Arctic (Minsley et al., 2012). MDV, as a system with brines beneath frozen ground and glacier ice, are potentially not unique in Antarctica, at least not in the subsurface. Parts of coastal Antarctica could have been flooded by seawater in the past, particularly with continental crust being depressed by the weight of glaciers (after Starinsky and Katz, 2003). The MDV are well explored due to the exposure of solid ground and proximity to McMurdo Station, a logistical hub for the United States Antarctic Program, but other areas farther afield and presently covered by glaciers could have similar widespread brines and may become targets for future AEM exploration. Understanding the hydrogeology of these coastal margins may be important for evaluating the impact of future climate warming on coastal Antarctica.

CONCLUSIONS

Using a helicopter-borne, time-domain EM sensor, we have quickly filled in major gaps in our understanding of subsurface geophysics in the MDV. Previous geophysical work in the area, much of it more than 40 years old, was performed at a few select locales, and the results were generalized to the whole region with no independent verification elsewhere. Our survey samples the MDV, particularly TV, at an unprecedented spatial scale relevant to a range of hydrological, glaciological, and geomorphic processes dominating this landscape. Data sets obtained by the localized past geophysical and borehole investigations serve as ground truths for our more regional AEM results. We find widespread areas of low-resistivity material at depth, indicating cryoconcentrated brines existing at subzero temperatures beneath unexpectedly thin frozen permafrost. The contiguous nature of these low-resistivity areas at depth and their connection with lakes on the surface suggests the presence of a regional-scale briny groundwater system. Such a system may function as an important pathway for long-term transport of chemicals in this slowly evolving landscape. It may also be capable of supporting microbial life, thereby greatly expanding the habitable zone in this high polar desert. On the upstream end of TV, our technique demonstrates that the subsurface hydrological connectivity extends directly from West Lake Bonney to the subglacial materials beneath TG at least as far upstream as the AEM system can penetrate the increasingly thick glacier ice. These two observations may require that researchers studying biogeochemistry of MDV lakes take into account the possibility of chemical fluxes between the groundwater system and lakes.

TEM surveys complement other geophysical techniques, especially radar. High-frequency radar is used for examining internal structure of near-surface features, and low-frequency radar can pen-

etrate deep, especially in polar glacier ice. However, a radar signal attenuates quickly in the presence of conductive fluids. Resistivity techniques can make measurements through liquid water, and in the case of brines, which are a common form of liquid water in the MDV, resistivity techniques can return information relevant to subsurface salinity and porosity. Extremely low resistivity brines limit the DOI of EM resistivity techniques, and thick ice cover can prevent the imaging of very deep brines, but this can be overcome by using higher moment systems. Advances in EM resistivity techniques will make it even more useful in the MDV and for exploration in similar settings in Antarctica and the Arctic. Due to the important similarities between the MDV and Mars, Antarctica is also a promising location where scientists can improve approaches toward studying subsurface brine systems on other planetary bodies.

ACKNOWLEDGMENTS

This material is based upon work supported by the National Science Foundation under grant no. 1344349 to S. Tulaczyk and 1344348, 1241503, and 1344348 to J. Mikucki. Invaluable field support was provided by Raytheon Polar Services and the PHI helicopter pilots. This manuscript benefited tremendously from the thoughtful input of D. Stillman and two anonymous reviewers. We also thank the editors at GEOPHYSICS for their support during the production of this manuscript.

REFERENCES

Archie, G., 1950, Introduction to petrophysics of reservoir rocks: AAPG, **34**, 943–961.

Arcone, S. A., 2002, Stratigraphic profiling with ground-penetrating radar in permafrost: A review of possible analogs for Mars: Journal of Geophysical Research, **107**, 5108, doi: 10.1029/2002JE001906.

Arcone, S. A., A. J. Delaney, and M. E. Prentice, 2000, Stratigraphic profiling in the Antarctic Dry Valleys: Proceedings of SPIE, **4084**, 772–777, doi: 10.1117/12.383514.

Arcone, S. A., and K. Kreutz, 2009, GPR reflection profiles of Clark and Commonwealth Glaciers, Dry Valleys, Antarctica: Annals of Glaciology, **50**, 121–129, doi: 10.3189/172756409789097531.

Auken, E., and A. V. Christiansen, 2004, Layered and laterally constrained 2D inversion of resistivity data: Geophysics, **69**, 752–761, doi: 10.1190/1.1759461.

Auken, E., A. V. Christiansen, C. Kirkegaard, G. Fiandaca, C. Schamper, A. Behroozmand, A. Binley, E. Nielsen, F. Effersø, N. B. Christensen, K. I. Sørensen, N. Foged, and G. Vignoli, 2014, An overview of a highly versatile forward and stable inverse algorithm for airborne, ground-based and borehole electromagnetic and electric data: Exploration Geophysics, **46**, 223–235, doi: 10.1071/EG13097.

Auken, E., A. V. Christiansen, J. H. Westergaard, C. Kirkegaard, N. Foged, and A. Viezzoli, 2009, An integrated processing scheme for high-resolution airborne electromagnetic surveys, the SkyTEM system: Exploration Geophysics, **40**, 184–192, doi: 10.1071/EG08128.

Berthling, I., B. Etzelmüller, K. Isaksen, and J. L. Sollid, 2000, Rock glaciers on Prins Karls Forland. II: GPR soundings and the development of internal structures: Permafrost and Periglacial Processes, **11**, 357–369, doi: 10.1002/1099-1530(200012)11:4<357::AID-PPP366>3.0.CO;2-6.

Bristow, C. S., P. C. Augustinus, I. C. Wallis, H. M. Jol, and E. J. Rhodes, 2010, Investigation of the age and migration of reversing dunes in Antarctica using GPR and OSL, with implications for GPR on Mars: Earth and Planetary Science Letters, **289**, 30–42, doi: 10.1016/j.epsl.2009.10.026.

Cartwright, K., and H. Harris, 1981, Hydrogeology of the Dry Valley region, *in* L. D. McGinnis, ed., Dry Valley Drilling Project: AGU.

Christiansen, A. V., and E. Auken, 2012, A global measure for depth of investigation: Geophysics, **77**, no. 4, WB171–WB177, doi: 10.1190/geo2011-0393.1.

Christiansen, A. V., E. Auken, and K. I. Sørensen, 2006, The transient electromagnetic method, *in* R. Kirsch, ed., Groundwater geophysics: A tool for hydrogeology: Springer, 179–225.

Christiansen, A. V., E. Auken, and A. Viezzoli, 2011, Quantification of modeling errors in airborne TEM caused by inaccurate system description: Geophysics, **76**, no. 1, F43–F52, doi: 10.1190/1.3511354.

Christner, B. C., J. C. Priscu, A. M. Achberger, C. Barbante, S. P. Carter, K. Christianson, A. B. Michaud, J. A. Mikucki, A. C. Mitchell, M. L. Skidmore, and T. J. Vick-Majors, and the WISSARD Science Team, 2014, A microbial ecosystem beneath the West Antarctic ice sheet: Nature, **512**, 310–313, doi: 10.1038/nature13667.

Creyts, T. T., and C. G. Schoof, 2009, Drainage through subglacial water sheets: Journal of Geophysical Research, **114**, F04008, doi: 10.1029/2008JF001215.

Decker, E. R., and G. Bucher, 1977, Geothermal studies in Antarctica: Antarctic Journal of the United States, **12**, 102–104.

Decker, E. R., and G. J. Bucher, 1982, Geothermal studies in the Ross Island-Dry Valley region, *in* C. Craddock, ed., Antarctic geoscience: The University of Wisconsin Press, 887–894.

Degenhardt, J. J., and J. R. Giardino, 2003, Subsurface investigation of a rock glacier using ground-penetrating radar: Implications for locating stored water on Mars: Journal of Geophysical Research: Planets, **108**, 8036, doi: 10.1029/2002JE001888.

Dickson, J. L., J. W. Head, J. S. Levy, and D. R. Marchant, 2013, Don Juan Pond, Antarctica: Near-surface $CaCl_2$-brine feeding Earth's most saline lake and implications for Mars: Scientific Reports, **3**, 1166, doi: 10.1038%2Fsrep01166.

Doran, P. T., C. P. McKay, G. D. Clow, G. L. Dana, A. G. Fountain, T. Nylen, and W. B. Lyons, 2002, Valley floor climate observations from the McMurdo dry valleys, Antarctica, 1986–2000: Journal of Geophysical Research, **107**, 4772, doi: 10.1029/2001JD002045.

Dugan, H. A., P. T. Doran, S. Tulaczyk, J. A. Mikucki, S. A. Arcone, E. Auken, C. Schamper, and R. A. Virginia, 2015a, Subsurface imaging reveals a confined aquifer beneath an ice-sealed Antarctic lake: Geophysical Research Letters, **42**, 96–103, doi: 10.1002/2014GL062431.

Dugan, H. A., P. T. Doran, B. Wagner, F. Kenig, C. H. Fritsen, S. A. Arcone, E. Kuhn, N. E. Ostrom, J. P. Warnock, and A. E. Murray, 2015b, Stratigraphy of Lake Vida, Antarctica: Hydrologic implications of 27 m of ice: The Cryosphere, **9**, 439–450, doi: 10.5194/tc-9-439-2015.

Engel, Z., D. Nývlt, and K. Láska, 2012, Ice thickness, areal and volumetric changes of Davies Dome and Whisky Glacier (James Ross Island, Antarctic Peninsula) in 1979–2006: Journal of Glaciology, **58**, 904–914, doi: 10.3189/2012JoG11J156.

Ferrians, O. J., R. J. Kachadoorian, and G. W. Greene, 1969, Permafrost and related engineering problems in Alaska: U.S. Geological Survey, Professional Paper 678.

Foged, N., E. Auken, A. V. Christiansen, and K. I. Sørensen, 2013, Test site calibration and validation of airborne and ground based TEM systems: Geophysics, **78**, no. 2, E95–E106, doi: 10.1190/geo2012-0244.1.

Foged, N., P. A. Marker, A. V. Christiansen, P. Bauer-Gottwein, F. Jørgensen, A.-S. Høyer, and E. Auken, 2014, Large-scale 3-D modeling by integration of resistivity models and borehole data through inversion: Hydrology and Earth System Sciences, **18**, 4349–4362, doi: 10.5194/hess-18-4349-2014.

Fukui, K., T. Sone, J. A. Strelin, C. A. Torielli, J. Mori, and Y. Fujii, 2008, Dynamics and GPR stratigraphy of a polar rock glacier on James Ross Island, Antarctic Peninsula: Journal of Glaciology, **54**, 445–451, doi: 10.3189/002214308785836940.

Gilichinsky, D., E. Rivkina, V. Shcherbakova, K. Laurinavichuis, and J. Tiedje, 2003, Supercooled water brines within permafrost: An unknown ecological niche for microorganisms: A model for astrobiology: Astrobiology, **3**, 331–341, doi: 10.1089/153110703769016424.

Gilichinsky, D. A., G. S. Wilson, E. I. Friedmann, C. P. McKay, R. S. Sletten, E. M. Rivkina, T. A. Vishnivetskaya, L. G. Erokhina, N. E. Ivanushkina, G. A. Kochkina, V. A. Shcherbakova, V. S. Soina, E. V. Spirina, E. A. Vorobyova, D. G. Fyodorov-Davydov, B. Hallet, S. M. Ozerskaya, V. A. Sorokovikov, K. S. Laurinavichyus, A. V. Shatilovich, J. P. Chanton, V. E. Ostroumov, and J. M. Tiedje, 2007, Microbial populations in Antarctic permafrost: Biodiversity, state, age, and implication for astrobiology: Astrobiology, **7**, 275–311, doi: 10.1089/ast.2006.0012.

Hall, B. L., G. H. Denton, and C. H. Hendy, 2000, Evidence from Taylor Valley for a grounded ice sheet in the Ross Sea, Antarctica: Geografiska Annaler: Series A, Physical Geography, **82**, 275–303.

Herut, B., A. Starinsky, A. Katz, and A. Bein, 1990, The role of seawater freezing in the formation of subsurface brines: Geochimica et Cosmochimica Acta, **54**, 13–21, doi: 10.1016/0016-7037(90)90190-V.

Holt, J. W., M. E. Peters, S. D. Kempf, D. L. Morse, and D. D. Blankenship, 2006, Echo source discrimination in single-pass airborne radar sounding data from the Dry Valleys, Antarctica: Implications for orbital sounding of Mars: Journal of Geophysical Research E: Planets, **111**, E06S24, doi: 10.1029/2005JE002525.

Hubbard, A., W. Lawson, B. Anderson, B. Hubbard, and H. Blatter, 2004, Evidence for subglacial ponding across Taylor Glacier, Dry Valleys, Antarctica: Annals of Glaciology, **39**, 79–84, doi: 10.3189/172756404781813970.

IPCC, 2007: Climate change 2007: The physical science basis, *in* S., Solomon, D. Qin, M. Manning, Z. Chen, M. Marquis, K. B. Averyt, M. Tignor, and H. L. Miller, eds., Contribution of Working Group I to the Fourth Assessment Report of the Intergovernmental Panel on Climate Change: Cambridge University Press.

Isaksen, K., R. S. Ødegård, T. Eiken, and J. L. Sollid, 2000, Composition, flow and development of two tongue-shaped rock glaciers in the permafrost of Svalbard: Permafrost and Periglacial Processes, **11**, 241–257, doi: 10.1002/1099-1530(200007/09)11:3<241::AID-PPP358>3.0.CO;2-A.

Jørgensen, F., W. Scheer, S. Thomsen, T. O. Sonnenborg, K. Hinsby, H. Wiederhold, C. Schamper, T. Burschil, B. Roth, R. Kirsch, and E. Auken, 2012, Transboundary geophysical mapping of geological elements and salinity distribution critical for the assessment of future sea water intrusion in response to sea level rise: Hydrology and Earth System Sciences, **16**, 1845–1862, doi: 10.5194/hess-16-1845-2012.

Joughin, I., R. B. Alley, and D. M. Holland, 2012, Ice-sheet response to oceanic forcing: Science, **338**, 1172–1176, doi: 10.1126/science.1226481.

Kamb, B., 1987, Glacier surge mechanism based on linked cavity configuration of the basal water conduit system: Journal of Geophysical Research, **92**, 9083–9100, doi: 10.1029/JB092iB09p09083.

Kavanaugh, J. L., and K. M. Cuffey, 2009, Dynamics and mass balance of Taylor Glacier, Antarctica. Part 2: Force balance and longitudinal coupling: Journal of Geophysical Research, **114**, F04011, doi: 10.1029/2009JF001329.

Keys, J., 1979, Saline discharge at the terminus of the Taylor Glacier: Antarctic Journal of the United States, **14**, 82–85.

Kirkegaard, C., and E. Auken, 2015, A parallel, scalable and memory efficient inversion code for very large-scale airborne EM surveys: Geophysical Prospecting, **63**, 495–507, doi: 10.1111/1365-2478.12200.

Kirkegaard, C., T. O. Sonnenborg, E. Auken, and F. Jørgensen, 2011, Salinity distribution in heterogeneous coastal aquifers mapped by airborne electromagnetics: Vadose Zone Journal, **10**, 125–135, doi: 10.2136/vzj2010.0038.

Kirsch, R., K.-P. Sengpiel, and W. Voss, 2003, The use of electrical conductivity mapping in the definition of an aquifer vulnerability index: Near Surface Geophysics, **1**, 13–19, doi: 10.3997/1873-0604.2002003.

Levy, J. S., A. G. Fountain, M. N. Gooseff, K. A. Welch, and W. B. Lyons, 2011, Water tracks and permafrost in Taylor Valley, Antarctica: Extensive and shallow groundwater connectivity in a cold desert ecosystem: Geological Society of America Bulletin, **123**, 2295–2311, doi: 10.1130/B30436.1.

Lyons, W. B., K. A. Welch, G. Snyder, J. Olesik, E. Y. Graham, G. M. Marion, and R. J. Poreda, 2005, Halogen geochemistry of the McMurdo dry valleys lakes, Antarctica: Clues to the origin of solutes and lake evolution: Geochimica et Cosmochimica Acta, **69**, 305–323, doi: 10.1016/j.gca.2004.06.040.

Mackay, S. L., D. R. Marchant, J. L. Lamp, and J. W. Head, 2014, Cold-based debris-covered glaciers: Evaluating their potential as climate archives through studies of ground-penetrating radar and surface morphology: Journal of Geophysical Research, **119**, 2505–2540, doi: 10.1002/2014JF003178.

McGinnis, L., K. Nakao, and C. Clark, 1973, Geophysical identification of frozen and unfrozen ground, Antarctica, *in* F. J. Sanger, ed., Proceedings of the 2nd International Conference on Permafrost, National Academy of Sciences, 136–146.

McGinnis, L. D., and T. E. Jensen, 1971, Permafrost-hydrogeologic regimen in two ice-free valleys, Antarctica, from electrical depth sounding: Quaternary Research, **1**, 389–409, doi: 10.1016/0033-5894(71)90073-1.

McGinnis, L. D., and D. R. Osby, 1977, Logging summary of Dry Valley Drilling Project: Antarctica Journal of the United States, **12**, 115–117.

McGinnis, L. D., D. R. Osby, and R. Kohout, 1982, Paleohydrology inferred from salinity measurements on Dry Valley Drilling Project cores from Taylor Valley, Antarctica, *in* C. Craddock, ed., Antarctic geoscience 4: University of Wisconsin Press, 1133–1138.

McGuire, A. D., L. G. Anderson, T. R. Christensen, S. Dallimore, L. D. Guo, D. J. Hayes, M. Heimann, T. D. Lorenson, R. W. Macdonald, and N. Roulet, 2009, Sensitivity of the carbon cycle in the Arctic to climate change: Ecological Monographs, **79**, 523–555, doi: 10.1890/08-2025.1.

McKelvey, B. C., 1975, DVDP sites 10 and 11, Taylor Valley: Dry Valley Drilling Project Bulletin, **5**, 16–60.

Mikucki, J. A., E. Auken, S. Tulaczyk, R. A. Virginia, C. Schamper, K. I. Sørensen, P. T. Doran, H. A. Dugan, and N. Foley, 2015, Deep groundwater and potential subsurface habitats beneath an Antarctic dry valley: Nature Communications, **6**, 6831, doi: 10.1038/ncomms7831.

Mikucki, J. A., C. C. M. Foreman, B. Sattler, W. B. Lyons, and J. C. Priscu, 2004, Geomicrobiology of Blood Falls: An iron-rich saline discharge at the terminus of the Taylor Glacier, Antarctica: Aquatic Geochemistry, **10**, 199–220, doi: 10.1007/s10498-004-2259-x.

Mikucki, J. A., A. Pearson, D. T. Johnston, A. V. Turchyn, J. Farquhar, D. P. Schrag, A. D. Anbar, J. C. Priscu, and P. A. Lee, 2009, A contemporary microbially maintained subglacial ferrous "ocean": Science, **324**, 397–400, doi: 10.1126/science.1167350.

Mikucki, J. A., and J. C. Priscu, 2007, Bacterial diversity associated with Blood Falls, a subglacial outflow from the Taylor Glacier, Antarctica: Applied and Environmental Microbiology, **73**, 4029–4039, doi: 10.1128/AEM.01396-06.

Minsley, B. J., J. D. Abraham, B. D. Smith, J. C. Cannia, C. I. Voss, M. T. Jorgenson, M. A. Walvoord, B. K. Wylie, L. Anderson, L. B. Ball, M. Deszcz-Pan, T. P. Wellman, and T. A. Ager, 2012, Airborne electromagnetic imaging of discontinuous permafrost: Geophysical Research Letters, **39**, L02503, doi: 10.1029/2011GL050079.

Osterkamp, T., and M. Jorgenson, 2009, Permafrost conditions and processes, *in* R. Young, and L. Norby, eds., Geological monitoring: Geological Society of America, 205–227.

Osterkamp, T. E., and C. R. Burn, 2003, Permafrost: Encyclopedia of Atmospheric Sciences 4, 1717–1729, doi: 10.1016/B0-12-227090-8/00311-0.

Palacky, G. J., 1987, Clay mapping using electromagnetic methods: First Break, **5**, 295–306, doi: 10.3997/1365-2397.1987015.

Paytan, A., A. L. Lecher, N. Dimova, K. J. Sparrow, F. G.-T. Kodovska, J. Murray, S. Tulaczyk, and J. D. Kessler, 2015, Methane transport from the active layer to lakes in the Arctic using Toolik Lake, Alaska, as a case study: Proceedings of the National Academy of Sciences, **112**, 3636–3640, doi: 10.1073/pnas.1417392112.

Pettit, E. C., E. N. Whorton, E. D. Waddington, and R. S. Sletten, 2014, Influence of debris-rich basal ice on flow of a polar glacier: Journal of Glaciology, **60**, 989–1006, doi: 10.3189/2014JoG13J161.

Poreda, R. J., A. G. Hunt, W. B. Lyons, and K. A. Welch, 2004, The helium isotopic chemistry of Lake Bonney, Taylor Valley, Antarctica: Timing of late Holocene climate change in Antarctica: Aquatic Geochemistry, **10**, 353–371, doi: 10.1007/s10498-004-2265-z.

Powell, R. D., 1981, Sedimentation conditions in Taylor Valley, Antarctica, inferred from textural analysis of DVDP Cores, *in* D. McGinnis, ed., Dry Valley Drilling Project: AGU, 331–349.

Schamper, C., E. Auken, and K. I. Sørensen, 2014, Coil response inversion for very early time modeling of helicopter-borne time-domain EM data and mapping of near-surface geological layers: Geophysical Prospecting, **62**, 658–674, doi: 10.1111/1365-2478.12104.

Shean, D. E., and D. R. Marchant, 2010, Seismic and GPR surveys of Mullins Glacier, McMurdo Dry Valleys, Antarctica: Ice thickness, internal structure and implications for surface ridge formation: Journal of Glaciology, **56**, 48–64, doi: 10.3189/002214310791190901.

Smith, R., 2014, Electromagnetic induction methods in mining geophysics from 2008 to 2012: Surveys in Geophysics, **35**, 123–156, doi: 10.1007/s10712-013-9227-1.

Sold, L., M. Huss, A. Eichler, M. Schwikowski, and M. Hoelzle, 2014, Recent accumulation rates of an alpine glacier derived from firn cores and repeated helicopter-borne GPR: The Cryosphere Discussion, **8**, 4431–4462, doi: 10.5194/tcd-8-4431-2014.

Sørensen, K. I., and E. Auken, 2004, SkyTEM — A new high-resolution helicopter transient electromagnetic system: Exploration Geophysics, **35**, 194–202, doi: 10.1071/EG04194.

Spigel, R. H., and J. C. Priscu, 1996, Evolution of temperature and salt structure of Lake Bonney, a chemically stratified Antarctic lake: Hydrobiologia, **321**, 177–190, doi: 10.1007/BF00143749.

Starinsky, A., and A. Katz, 2003, The formation of natural cryogenic brines: Geochimica et Cosmochimica Acta, **67**, 1475–1484, doi: 10.1016/S0016-7037(02)01295-4.

Stuiver, M., I. C. Yang, G. H. Denton, and T. B. Kellogg, 1981, Oxygen isotope ratios of Antarctic permafrost and glacier ice, *in* D. McGinnis, ed., Dry Valley Drilling Project, AGI, 131–139.

Sugden, D., G. Denton, and D. Marchant, 1995, Landscape evolution of the Dry Valleys, Transantarctic Mountains: Tectonic implications: Journal of Geophysical Research, **100**, 9949–9968, doi: 10.1029/94JB02875.

Teatini, P., L. Tosi, A. Viezzoli, L. Baradello, M. Zecchin, and S. Silvestri, 2011, Understanding the hydrogeology of the Venice Lagoon subsurface with airborne electromagnetics: Journal of Hydrology, **411**, 342–354, doi: 10.1016/j.jhydrol.2011.10.017.

Toner, J. D., and R. S. Sletten, 2013, The formation of Ca-Cl-rich groundwaters in the Dry Valleys of Antarctica: Field measurements and modeling of reactive transport: Geochimica et Cosmochimica Acta, **110**, 84–105, doi: 10.1016/j.gca.2013.02.013.

Toner, J. D., R. S. Sletten, and M. L. Prentice, 2013, Soluble salt accumulations in Taylor Valley, Antarctica: Implications for paleolakes and Ross Sea Ice Sheet dynamics: Journal of Geophysical Research: Solid Earth, **118**, 198–215, doi: 10.1029/2012JF002467.

Viezzoli, A., A. V. Christiansen, E. Auken, and K. I. Sørensen, 2008, Quasi-3D modeling of airborne TEM data by spatially constrained inversion: Geophysics, **73**, no. 3, F105–F113, doi: 10.1190/1.2895521.

Vignoli, G., G. Fiandaca, A. V. Christiansen, C. Kirkegaard, and E. Auken, 2015, Sharp spatially constrained inversion with applications to transient

electromagnetic data: Geophysical Prospecting, **63**, 243–255, doi: 10.1111/1365-2478.12185.

Wadham, J. L., S. Arndt, S. Tulaczyk, M. Stibal, M. Tranter, J. Telling, G. P. Lis, E. Lawson, A. Ridgwell, A. Dubnick, M. J. Sharp, A. M. Anesio, and C. E. H. Butler, 2012, Potential methane reservoirs beneath Antarctica: Nature, **488**, 633–637, doi: 10.1038/nature11374.

Wadham, J. L., R. De'ath, F. M. Monteiro, M. Tranter, A. Ridgwell, R. Raiswell, and S. Tulaczyk, 2013, The potential role of the Antarctic ice sheet in global biogeochemical cycles: Earth and Environmental Science Transactions of the Royal Society of Edinburgh, **104**, 55–67, doi: 10.1017/S1755691013000108.

Wadham, J. L., M. Tranter, S. Tulaczyk, and M. Sharp, 2008, Subglacial methanogenesis: A potential climatic amplifier?: Global Biogeochemical Cycles, **22**, GB2021, doi: 10.1029/2007GB002951.

Ward, S. H., and G. W. Hohmann, 1988, Electromagnetic theory for geophysical applications, *in* M. N. Nabighian, ed., Electromagnetic methods in applied geophysics: SEG, 130–311.

Willis, M. J., B. G. Herried, M. G. Bevis, and R. E. Bell, 2015, Recharge of a subglacial lake by surface meltwater in northeast Greenland: Nature, **518**, 223–227., doi: 10.1038/nature14116.

Winberry, J. P., S. Anandakrishnan, D. A. Wiens, R. B. Alley, and K. Christianson, 2011, Dynamics of stick-slip motion, Whillans Ice Stream, Antarctica: Earth and Planetary Science Letters, **305**, 283–289, doi: 10.1016/j.epsl.2011.02.052.

Zimov, S., E. Schuur, and F. Chapin, 2006, Permafrost and the global carbon budget: Science, **312**, 1612–1613, doi: 10.1126/science.1128908.

Queries

1. SEG style requires that URLs "www.mcmlter.org" and "www.hgg.au.dk" are made into references in the reference list instead of listed in the text. Please provide the author/institution, web page name, accessed date and the year of the web page.

2. Please provide an in-text citation for the references Willis et al. (2015), Mikucki et al. (2004), and McKelvey (1975), or may we delete them?

3. Please provide complete reference-list details for the citations Zhdanov (2009), Hendy (2000), and Sharma (1997), or may we delete them?

4. Please clarify should this be Dugan et al. (2015a) or (2015b).

5. Can we delete the outer box in Table 2, as per style?

6. Please provide the page range for Cartwright and Harris (1981).

7. Please provide the page range for IPCC (2007).

Funding Information

The following agencies have been identified as providing funding for your article. Please review the information carefully. If any changes are required, please submit those along with your other corrections to this article.

- National Science Foundation (FundRef Registry ID: http://dx.doi.org/10.13039/100000001)